Silylation of Single-Walled Carbon Nanotubes

Tirandai Hemraj-Benny† and Stanislaus S. Wong*,†,‡

Department of Chemistry, State University of New York at Stony Brook, Stony Brook, New York 11794-3400, and Materials and Chemical Sciences Department, Brookhaven National Laboratory, Building 480, Upton, New York 11973

Received May 19, 2006. Revised Manuscript Received July 14, 2006

Herein we present, to the best of our knowledge, the first report of effective silylation of raw, pristine single-walled carbon nanotubes (SWNTs). Specifically, commercially available CoMoCAT SWNTs were functionalized at their ends and sidewalls (a) with trimethoxysilane and in a separate experiment, (b) with hexaphenyldisilane. Raman analyses demonstrated selective reactivity of predominantly smaller-diameter semiconducting nanotubes. High-resolution transmission electron microscopy (HRTEM), scanning electron microscopy, and atomic force microscopy showed that the functionalization reaction was structurally nondestructive to the tube integrity. Fourier transform infrared (FT-IR) spectroscopy, nuclear magnetic resonance (^{29}Si NMR) spectroscopy, X-ray photoelectron spectroscopy (XPS), and energy-dispersive X-ray spectroscopy (EDS) data provided evidence for chemical attachment of organosilanes onto the carbon nanotube surface. UV−visible data also yielded evidence for selectivity and functionalization.

Introduction

Single-walled carbon nanotubes (SWNTs) possess unique structural, electronic, mechanical, and optical properties.[1,2] The combination of the helicity and diameter of SWNTs, defined by the roll-up vector, that is, tube chirality, determines whether a tube is a metal or a semiconductor. One main motivation of understanding the electronic structure of carbon nanotubes is that as spatially constrained one-dimensional structures, they are the smallest dimensional systems that can be used for the efficient transport of electrons and optical excitations and, hence, are expected to be particularly important in the construction and integration of nanoscale devices.

The majority of electronics applications specifically require the isolation of semiconducting tubes.[3−6] However, the lack of control over the electronic properties of as-prepared nanotubes, for example, the inability to reliably separate masses of semiconducting from metallic tubes, has created a major stumbling block for their incorporation into functional devices. Thus, there is an urgent need to obtain electronic monodispersity in nanotube samples. Generating such monodisperse samples of nanotubes should also allow for detailed studies of diameter and chirality dependence of many different structural properties that are of fundamental interest in low-dimensional science.

One solution to this problem involves the controllable use of covalent chemistry to modify the sidewall surfaces of tubes to enhance the relative populations of either metallic or semiconducting tubes. Some of these types of functionalization reactions, such as osmylation and diazotization,[7−9] involve extraction of electrons from the nanotube itself. In particular, with these reactions, metallic SWNTs, due to their finite and readily available electron density at the Fermi level, are better able to stabilize the transition state involved, will consequently accelerate the forward rate of reaction, and, hence, will preferentially react as compared with semiconducting tubes. A particularly interesting means of altering the relative distribution of metallic versus semiconducting carbon nanotubes, which we have begun to explore, involves the chemical derivatization of nanotubes with a high κ dielectric coating material, such as Si-containing species.

Prior work on coating SWNTs with SiO_2 and analogous derivatives has focused on a number of methods. An early study[10] reported on the use of a promoter layer, 3-aminopropyltriethoxysilane, followed by a modified Stöber reaction to generate silica. Peptides have been used to both suspend SWNTs as well as direct the precipitation of silica onto their surfaces.[11] Treatment of a dispersion of SWNTs in an aqueous surfactant solution with an acidic solution of fumed

* To whom correspondence should be addressed. Phone: 631-632-1703, 631-344-3178. E-mail: sswong@notes.cc.sunysb.edu, sswong@bnl.gov.
† State University of New York at Stony Brook.
‡ Brookhaven National Laboratory.

(1) Dresselhaus, M. S.; Dresselhaus, G.; Avouris, P. *Carbon Nanotubes: Synthesis, Structure, Properties, and Applications*; Springer-Verlag: Berlin, 2001.
(2) Falvo, M. R.; Clary, G. J.; Taylor, R. M., II; Chi, V.; Brooks, F. P., Jr.; Washburn, S.; Superfine, R. *Nature* **1997**, *389*, 582.
(3) Bachtold, A.; Hadley, P.; Nakanishi, T.; Dekker, C. *Science* **2001**, *294*, 1317.
(4) Baughman, R. H.; Zakhidov, A. A.; de Heer, W. A. *Science* **2002**, *297*, 787.
(5) (a) Wong, S. S.; Joselevich, E.; Woolley, A. T.; Cheung, C. L.; Lieber, C. M. *Nature* **1998**, *394*, 52. (b) Banerjee, S.; Hemraj-Benny, T.; Wong, S. S. *J. Nanosci. Nanotech.* **2005**, *5*, 841.
(6) Yang, C.-M.; Kanoh, H.; Kaneko, K.; Yudasaka, M.; Iijima, S. *J. Phys. Chem. B* **2002**, *106*, 8994.
(7) Bahr, J. L.; Yang, J.; Kosynkin, D. V.; Broniskowski, M. J.; Smalley, R. E.; Tour, J. M. *J. Am. Chem.* Soc. **2001**, *123*, 6536.
(8) Banerjee, S.; Wong, S. S. *J. Am. Chem. Soc.* **2004**, *126*, 2073.
(9) Dyke, C. A.; Tour, J. M. *Nano Lett.* **2003**, *3*, 1215.
(10) Fu, Q.; Lu, C.; Liu, J. *Nano Lett.* **2002**, *2*, 329.

10.1021/cm061185x CCC: $33.50
Published on Web 09/02/2006

Scheme 1. Representation of Typical Reactions between SWNTs and Appropriate Silane Precursors

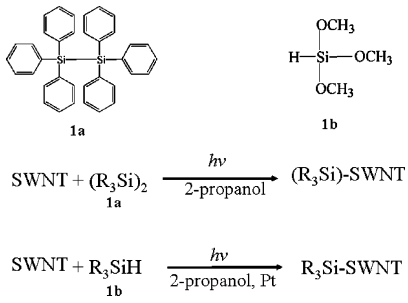

silica resulted in silica-coated SWNTs,[12] whereas a complementary method for generating silica-coated SWNTs was devised using a basic solution of aqueous sodium silicate.[13] Finally, the same group coated SWNTs with fluorine-doped silica by liquid-phase deposition using a silica/H_2SiF_6 solution in the presence of surfactant.[12]

We have embarked on a different strategy, inspired by theoretical studies[14,15] claiming that the [2+1] cycloaddition of silylene on nanotube sidewalls is site-selective, occurring preferentially on the 1,2-pair site and favoring opened structures.[16,17] Organosilanes have been extensively used as coupling agents on hydroxylated surfaces for generating organic coatings,[18] with the idea that the electrical properties of carbon nanotubes can be appropriately adjusted through rational chemical functionalization. In previous work, the silylation of oxidized multiwalled carbon nanotubes has been performed with a variety of reagents including *tert*-butylchlorodimethylsilane and 1-(*tert*-butyldimethylsilyl)imidazole.[19,20]

In the current study, we have chosen to investigate the silylation of pristine, unoxidized SWNTs. What is novel about this work is that this reaction is not spatially limited to defect sites and ends. Moreover, our silylation protocol does not require harsh oxidative methods. In fact, we have chosen to explore the photochemical silylation of SWNTs, a reaction analogous to that involving fullerenes.[21] It is hypothesized that the reaction scheme of the silylation of SWNTs is similar to that of fullerenes, as shown in Scheme 1. However, the chemical reactivity of these two carbonaceous systems likely differs. That is, whereas in fullerenes, the relief of the pyramidalization strain energy results in addition reactions being energetically favorable, in the case of SWNTs, π-orbital misalignment is expected to have a greater influence.[22] This misalignment, associated with bonds at an angle to the tube circumference, is the origin of torsional strain in nanotubes, and relief of this strain controls the extent to which addition reactions occur with nanotubes. Moreover, it is expected that smaller-diameter tubes would be more reactive than larger-diameter tubes because π-orbital misalignment as well as pyramidalization scale inversely with tube diameter.[23−25]

Herein we present, to the best of our knowledge, the first report of silylation of raw, pristine SWNTs. Specifically, commercially available CoMoCAT SWNTs were sidewall-functionalized (a) with trimethoxysilane and in a separate experiment, (b) with hexaphenyldisilane. Raman analyses demonstrated selective reactivity of smaller-diameter semiconducting nanotubes. Fourier transform infrared (FT-IR) spectroscopy, nuclear magnetic resonance (^{29}Si NMR) spectroscopy, X-ray photoelectron spectroscopy (XPS), and energy-dispersive X-ray spectroscopy (EDS) data provided evidence for chemical attachment of organosilanes onto the carbon nanotube surface. UV−visible data also yielded evidence for selectivity and functionalization.

In addition, several microscopy techniques, including atomic force microscopy (AFM), high-resolution transmission electron microscopy (HRTEM), and scanning electron microscopy (SEM), were used to determine the degree of nanotube purity and functionalization. Most importantly, these structural characterization techniques confirmed that silylation does not result in any noticeable form of destruction to the nanotube surface. Moreover, it was noted, upon silylation, that the solubility and stability of the SWNTs increased dramatically in dimethylformamide (DMF) as compared with pristine, unfunctionalized CoMoCAT nanotubes.

Experimental Section

Pretreatment of SWNTs. To ensure that the starting material, namely the unreacted SWNTs, were free of silicon, a known purification method[26] was used to initially treat the tubes. Specifically, a sample of commercially available nanotubes (SouthWest Nanotechnologies, Inc.) was suspended in a 0.2 M NaOH solution, while stirring for 24 h at 65 °C. Upon filtration through a polycarbonate 0.2 μm membrane, the remaining solid was washed with deionized water until the pH was neutral. The sample was subsequently allowed to dry overnight in a desiccator.[27] SEM and HRTEM images as well as EDS data (Figures 1 and 2) confirm that the starting material was free from any form of silicon. We refer to these samples in this manuscript as "SWNT starting materials".

(11) Pender, M. J.; Hartgerink, J. D.; Marujama, B.; Naik, R. R.; Stone, M. O.; Vaia, R. A. *Polym. Prepr. (Am. Chem. Soc., Div. Polym. Chem.)* **2005**, *46*, 83.
(12) (a) Whitsitt, E. A.; Moore, V. C.; Smalley, R. E.; Barron, A. R. *J. Mater. Chem.* **2005**, *15*, 4678. (b) Whitsitt, E. A.; Barron, A. R. *Nanoletters* **2003**, *3*, 775.
(13) Colorado, R., Jr.; Diosomito, M. E.; Barron, A. R. *Adv. Mater.* **2005**, *17*, 1634.
(14) Lu, X.; Tian, F.; Zhang, Q. *J. Phys. Chem. B* **2003**, *107*, 8388.
(15) Chu, Y. Y.; Su, M. D. *Chem. Phys. Lett.* **2004**, *394*, 231.
(16) Zhang, C.; Li, R.; Shang, Z.; Li, J.; Xing, Y.; Pan, Y.; Cai, Z.; Zhao, X. *J. Mol. Struct. (THEOCHEM)* **2004**, *681*, 225.
(17) Lu, J.; Nagase, S.; Zhang, X.; Maeda, Y.; Wakahara, T.; Nakahodo, T.; Tsuchiya, T.; Akasaka, T.; Yu, D.; Gao, Z.; Han, R.; Ye, H. *J. Mol. Struct. (THEOCHEM)* **2005**, *725*, 255.
(18) Duchet, J.; Chabert, B.; Chapel, J. P.; Gerard, J. F.; Chovelon, J. M.; Jaffrezic-Renault, N. *Langmuir* **1997**, *13*, 2271.
(19) Velasco-Santos, C.; Martinez-Hernandez, A. L.; Lozada-Cassou, M.; Alvarez-Castillo, A.; Castano, V. M. *Nanotechnology* **2002**, *13*, 495.
(20) Vast, L.; Philippin, G.; Destree, A.; Moreau, N.; Fonseca, A.; Nagy, J. B.; Delhalle, J.; Mekhalif, Z. *Nanotechnology* **2004**, *15*, 781.
(21) Akasaka, T.; Suzuki, T.; Maeda, Y.; Ara, M.; Wakahara, T.; Kobayashi, K.; Nagase, S.; Kako, M.; Nakadaira, T.; Fujitsuka, M.; Ito, O. *J. Org. Chem.* **1999**, *64*, 566.
(22) Haddon, R. C. *Acc. Chem. Res.* **1988**, *21*, 243.
(23) Niyogi, S.; Hamon, M. A.; Hu, H.; Zhao, B.; Bhowmik, P.; Sen, R.; Itkis, M. E.; Haddon, R. C. *Acc. Chem. Res.* **2002**, *35*, 1105.
(24) Hamon, M. A.; Itkis, M. E.; Niyogi, S.; Alvaraez, T.; Kuper, C.; Menon, M.; Haddon, R. C. *J. Am. Chem. Soc.* **2001**, *123*, 11292.
(25) Chen, Z.; Thiel, W.; Hirsch, A. *Chem. Phys. Chem.* **2003**, *4*, 93.
(26) Alvarez, W. E.; Pompeo, F.; Herrera, J. E.; Balzano, L.; Resasco, D. E. *Chem. Mater.* **2002**, *14*, 1853.
(27) Herrera, J. E.; Balzano, L.; Pompeo, F.; Resasco, D. E. *J. Nanosci. Nanotechnol.* **2003**, *3*, 133.

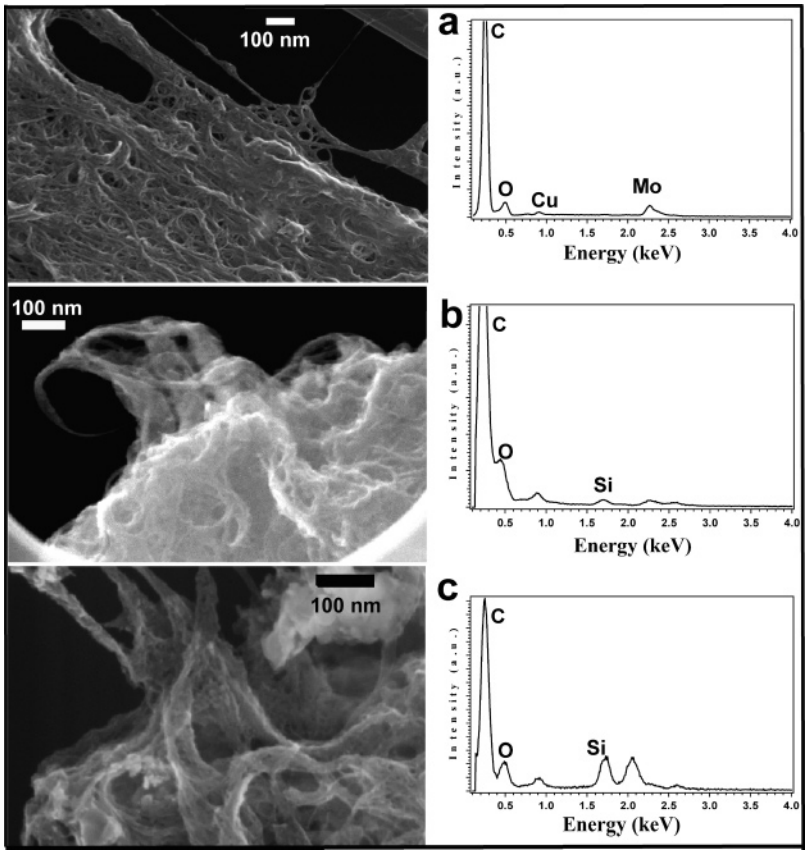

Figure 1. SEM images and EDS data for (a) SWNT starting material; (b) hexaphenyldisilane−SWNT adducts; and (c) trimethoxysilane−SWNT adducts. The copper signal originates from the sample grid, and the molybdenum signal arises from the catalyst used to synthesize the nanotube.

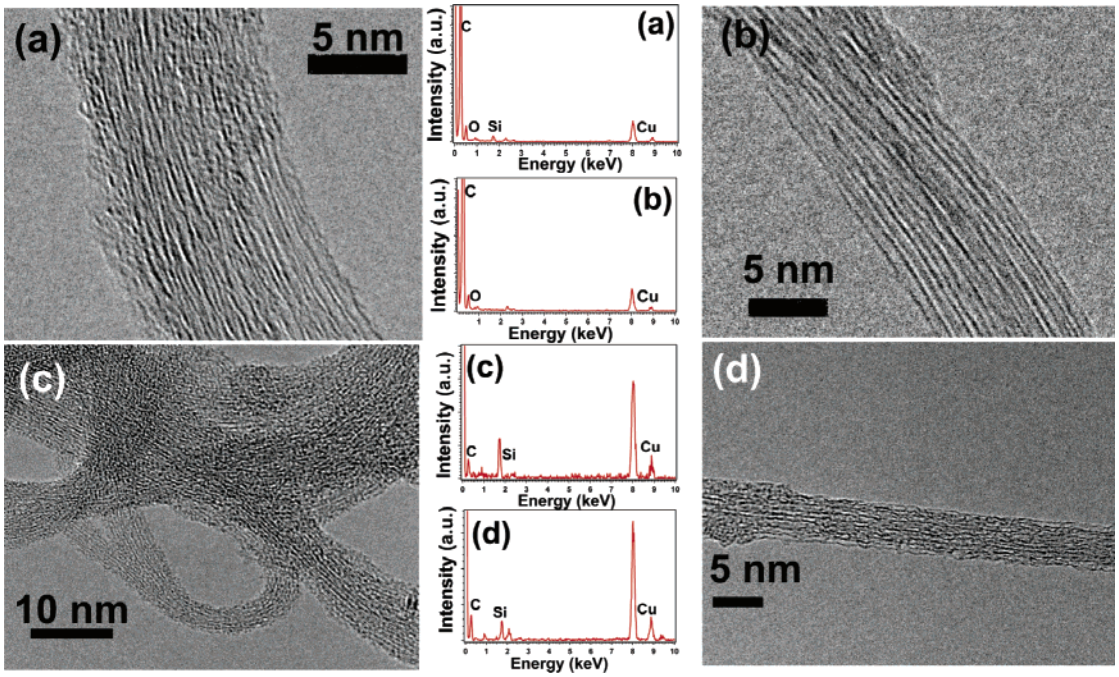

Figure 2. HRTEM and EDS data for (a) pristine CoMoCAT SWNT starting materials; (b) control samples; (c) hexaphenyldisilane−SWNT adducts; and (d) trimethoxysilane−SWNT adducts.

Control Experiment. To better understand the effect of only UV irradiation on the tube surface, a sample of base-treated SWNTs was placed in 2-propanol and was allowed to stir for 48 h with exposure to the UV lamp. HRTEM data (Figure 2b) confirm that there was no visible damage occurring on tube sidewalls. In addition, Raman data taken on this sample were compared with that obtained on silane adducts. Our results confirm that observed changes in the Raman data were likely due to the functionalization reaction as opposed to any process associated with lamp irradiation. We refer to these samples in this manuscript as "controls".

Silylation of SWNTs. A rectangular quartz holder, containing ~40 mg of dried SWNTs in the presence of extra dry 2-propanol (Aldrich), was flushed continuously with argon. The whole setup was sealed within a Schlenk setup to avoid the presence of moisture.

The tubes were gently dispersed by sonication for a few seconds after which vigorous stirring was performed.

(a) For the reaction with hexaphenyldisilane, 50 mg of the silane precursor was inserted into a Schlenk flask (flushed with argon) to which 20 mL of extra dry 2-propanol was then added. Upon dissolution, this solution was then combined with the SWNT dispersion. Although it may not have been completely necessary for the hexaphenyldisilane reaction to have been performed in the absence of water, as in the case with fullerenes,[21] the above precautions were taken to ensure a more controlled environment. Irradiation of the mixture with a 500 W mercury xenon lamp for 48 h was subsequently performed. The functionalized adduct was isolated by filtering the mixture over a 0.2 μm polycarbonate membrane, after which the remaining solid was washed several times with 2-propanol and distilled water to remove any unreacted organosilane precursor.

(b) In the case of trimethoxysilane, use of a hydrogen hexachloroplatinate(IV) hexahydrate (38−40% Pt) catalyst was the main modification in a reaction protocol similar to that reported for hexaphenyldisilane. In this case, the catalyst solution was initially added to a stirred solution of SWNTs, after which the organosilane precursor (trimethoxysilane, 0.016 mol) was inserted. The entire process was performed under Schlenk conditions to ensure the absence of moisture in the system. After irradiation for 48 h, filtration followed by washing and drying was performed to isolate the functionalized adduct.

Solubility. Solubility tests were performed in DMF. The trimethoxysilane−SWNT adduct was found to maintain a solubility value of ∼1 mg/mL whereas the hexaphenyldisilane−SWNT adduct, pristine CoMoCAT SWNTs, and control materials all showed solubilities less than 0.4 mg/mL. Most importantly, solutions of trimethoxysilane−SWNT adducts remained stable for more than 7 months, whereas solutions of all of the other samples precipitated within hours. Images of solutions and dispersions of all of these samples are shown in Supporting Information.

Spectroscopy. FT-IR data were obtained on a Nexus 670 (Thermo Nicolet) equipped with a single reflectance ZnSe ATR accessory in addition to a KBr beam splitter and a DTGS KBr detector for mid-IR as well as a CaF_2 beam splitter and an InGaAs detector for near-IR. Powder samples were placed onto a ZnSe crystal where data were taken with a reproducible pressure. Background corrections with the ZnSe crystal were performed in both ranges.

UV−visible spectra were collected on a Thermospectronics UV1 instrument using quartz cells possessing a 10 mm path length at a resolution of 1 nm. Samples were sonicated in DMF for 10−30 min and were subsequently centrifuged. Pristine CoMoCAT samples were sonicated for the longer time periods to ensure solubility. The supernatant decants were collected and diluted to approximately the same absorption intensity, for comparative purposes, at a wavelength of 900 nm prior to spectral acquisition.

Raman spectra were obtained on solid samples dispersed in ethanol and placed onto a Si wafer. Spectra were obtained on a Renishaw 1000 Raman microspectrometer with excitation from argon ion (514.5 nm), He−Ne (632.8 nm), and diode (780 nm) lasers, respectively. In addition, a Renishaw System 1000 microscope with a tunable argon ion laser was used to acquire Raman data at 488 nm excitation. A 50× objective and low laser power density were used for the irradiation of the sample and for signal collection. The laser power was kept sufficiently low to avoid heating of the samples by optical filtering and/or defocusing of the laser beam at the sample surface. Spectra were collected in the range of 3000−100 cm^{-1} with a resolution of 1 cm^{-1}.

^{29}Si NMR spectra were recorded at room temperature on a Brüker solid state spectrometer operating at 149.05 MHz for ^{29}Si. A typical ^{29}Si path length of 5 μs was used, and varying numbers of scans (depending on the sample involved) were performed. Powdered samples were placed in 4 mm rotor sample holders.

In collecting the XPS data, pressed wafers of the samples were attached to a stainless steel holder using conductive double-sided carbon tape which was then installed in the vacuum chamber of a model DS800 XPS surface analysis system manufactured by Kratos Analytical Plc (Manchester, U.K.). The chamber was evacuated to a base pressure of $\sim 5 \times 10^{-9}$ Torr. A hemispherical energy analyzer was used for electron detection. XPS spectra were collected using a Mg Kα X-ray source, at an 80 eV pass energy, and in 0.75 eV steps for each sample survey spectrum. Collected spectra were plotted and used to generate estimates of the atomic and weight concentrations of the elements, as indicated by peaks present in the spectral data (Supporting Information). High-resolution spectra were collected for the major elements detected to study relevant chemical bonding structures. These data were obtained at a pass energy of 40 eV and in 0.1 eV steps. High-resolution data were subsequently peak-fitted, plotted, and tabulated to illustrate the chemical species present for each major element detected (Supporting Information).

Microscopy. HRTEM images, as well as EDS data, were obtained on a JEOL 2010F high-resolution transmission electron microscope, equipped with an Oxford INCA EDS system, at an accelerating voltage of 200 kV. Samples were prepared by drying sample droplets from an ethanolic dispersion onto a 300-mesh Cu grid coated with a lacey carbon film. Prior to deposition, this dispersion was briefly sonicated for 10 s to ensure a uniform, homogeneous concentration of the carbon nanotubes within the solution.

Samples for SEM were studied using a field-emission scanning electron microscope (FE-SEM Leo 1550 with EDS capabilities), operating at accelerating voltages of 2−10 kV at a 2 mm working distance. In fact, these samples were drop dried onto 300 mesh Cu grids and held over a Be plate inside a homemade sample holder.

AFM height images were acquired in tapping mode in air at resonant frequencies of 50−75 kHz with oscillating amplitudes of 10−100 nm. The samples were dispersed in DMF, spin coated onto a freshly cleaved highly oriented pyrolytic graphite substrate, and finally imaged with Si tips (force modulation etched silicon probes, Nanoworld (k = 3−6 N/m)) using a Multimode Nanoscope IIIa (Digital Instruments, Santa Barbara, CA).

Results and Discussion

Electron Microscopy. SEM images of SWNT starting materials, trimethoxysilane−SWNT adducts, and hexaphenyldisilane−SWNT adducts are shown in Figure 1, along with their respective EDS data. It is evident that the initial starting material, consisting of a dense "spaghetti" mat of nanotubes, was indeed very pure and relatively free from amorphous carbon and silica impurities. The absence of silica impurities in the starting material was also confirmed by XPS and EDS analyses performed on these samples. Bundles of SWNTs were observed, ranging in size from ∼4−20 nm in diameter, in addition to the presence of individual tubes of ∼1 nm diameter. It is evident from the images obtained for both types of functionalized adducts, Figure 1b,c, that a layer of coating formed on the surfaces of bundles of these tubes as well as on those of single tubes. From EDS data, the

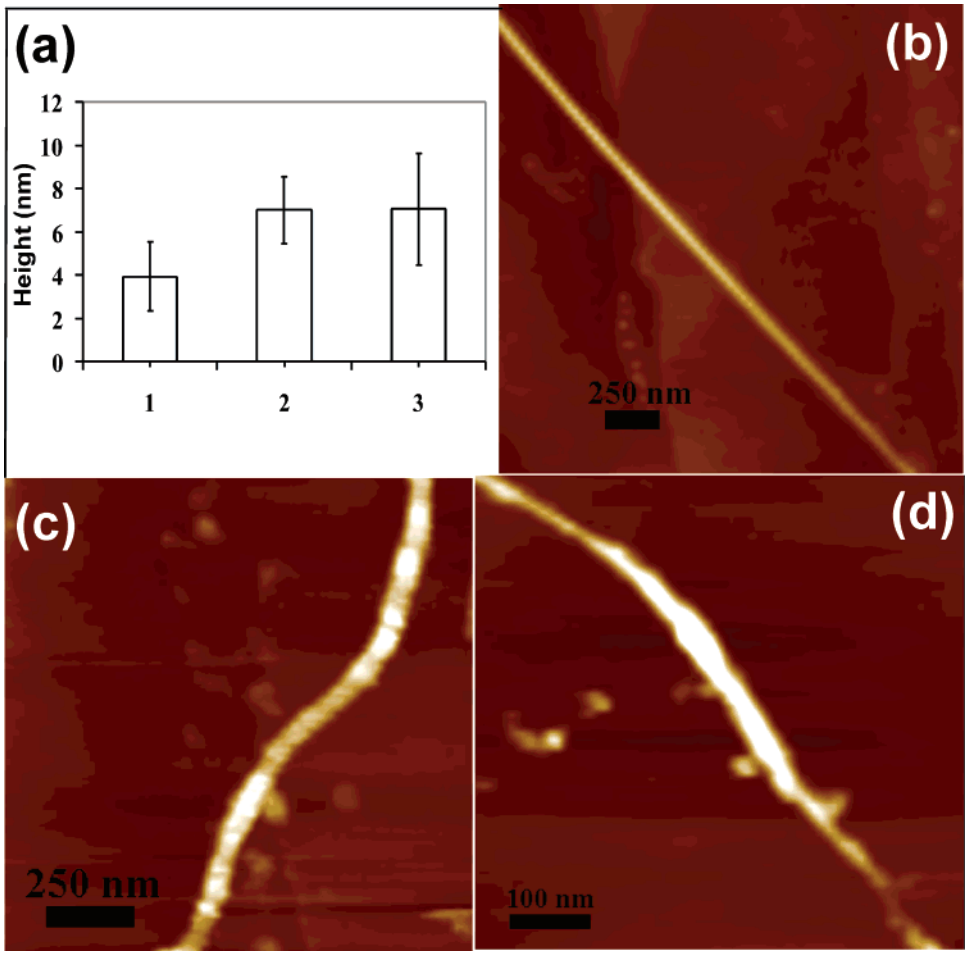

Figure 3. AFM analysis. (a) Heights of various nanotube samples: (1) SWNT starting material, 3.92 ± 1.58 nm; (2) trimethoxysilane−SWNT adducts, 6.99 ± 1.53 nm; (3) hexaphenyldisilane−SWNT adducts, 7.03 ± 2.56 nm. AFM height images of (b) SWNT starting materials, of (c) hexaphenyldisilane−SWNT adducts, and of (d) trimethoxysilane−SWNT adducts.

presence of silica was noted on these derivatized adducts, hypothesized to have originated from the presence of attached organosilane precursors.

It is also plausible from collected SEM images that the nanotubes retained their structural features and were not obviously damaged by the silylation process itself. This assertion was also further confirmed by HRTEM. Figure 2 shows images of pristine CoMoCAT SWNTs, of controls, and of the two functionalized adducts, respectively. From the EDS analysis, the starting material of this particular reaction, namely purified, base-treated nanotubes, was effectively free of any form of silicon. After the reaction (Figure 2c,d), it is clear that silicon was in fact present on localized areas of the tubes in the form of a coating on the nanotube surface. Moreover, it should be noted that the tubes were neither damaged by the base treatment nor damaged by UV lamp irradiation, as shown in the control experiment data as well as in the functionalized nanotube results.

AFM. To determine the precise thickness of the tube coating, a systematic AFM height analysis was undertaken, with averaged height measurements based on >35 bundles of tubes per sample. According to Figure 3, there is a clear observed increase in thickness of both adducts relative to that of pristine, unreacted nanotubes, which could not be ascribed to nanotube aggregation effects alone. Specifically, the trimethoxysilane−SWNT adduct consisted of a coating with dimensions of 6.99 ± 1.53 nm. The hexaphenyldisilane−SWNT adduct was covered with a layer measuring 7.03 ± 2.56 nm. By contrast, the SWNT starting material possessed an averaged height of 3.92 ± 1.58 nm. We noted a more continuous coating for trimethoxysilane−SWNT adducts as compared with hexaphenyldisilane−SWNT adducts. Nonetheless, it is unreasonable to expect that every single nanotube will be completely coated because this reaction was carried out on a combination of individual as well as bundles of tubes. That is, we would expect to see images of nonuniformly functionalized tubes, consisting of localized areas of derivatization exposed by sonication during sample preparation for AFM analysis. In fact, such an unevenly derivatized nanotube structure, manifested as the observation of uneven, disparate heights along selected cross sections distributed along the length of the sample, is observed in Figure 3d.

Nevertheless, the point that should be emphasized is that the regions of the nanotube, functionalized with the trimethoxysilane precursor, consisted of a continuous, homogeneous coating, which was effectively uniform in height along the length of the structure. Thus, one can envision complete surface functionalization with this particular reaction on a single individual tube. Images observed for the hexaphenyldisilane−SWNT adduct, shown in Figure 3c, demonstrated functionalization along the nanotube sidewalls

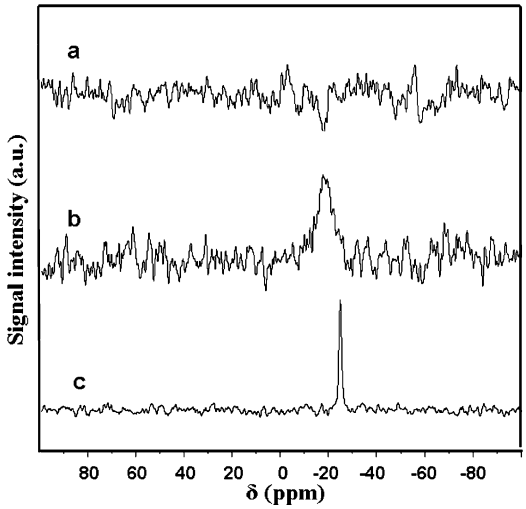

Figure 4. ^{29}Si NMR spectroscopy of (a) SWNT starting materials, (b) hexaphenyldisilane−SWNT adducts, and (c) the hexaphenyldisilane precursor.

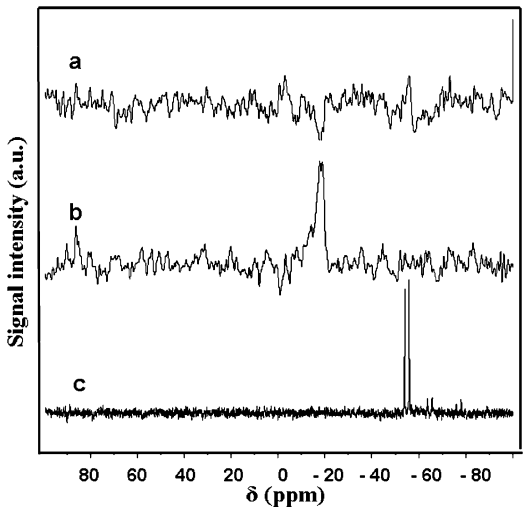

Figure 5. ^{29}Si NMR spectroscopy of (a) SWNT starting materials, (b) trimethoxysilane−SWNT adducts, and (c) the trimethoxysilane precursor.

but with less uniformity. As a comparison, unreacted tubes are shown in Figure 3b.

Silicon NMR Spectroscopy. Solid-state ^{29}Si NMR spectroscopy was used to characterize the attachment of organosilane precursors to the SWNT surfaces. As noted in the spectra, in Figures 4a and 5a, a signal was not detected for the raw, pristine SWNT starting material. Rather, a sharp signal was seen at −25 ppm for the hexaphenyldisilane precursor (Figure 4c), which was also previously observed by prior literature.[28,29] Upon attachment to the carbon nanotube, this peak shifted downfield to a higher frequency of −18 ppm and also broadened. Thus, it may be inferred that although the molecular precursor is likely still present, it is no longer present in its original coordination mode. The nature of the neighboring electronic environment around the Si atom likely altered only slightly though as the chemical shift was on the order of 7 ppm. This observation is consistent with the conversion of a Si−Si bond in the original precursor to a Si−C bond in its coordinative formulation with the carbon nanotube itself. An increase in peak width of the NMR peak is indicative of the localization and immobilization, through restriction of the degrees of conformational freedom, of Si-containing moieties onto surface sites of the tube with an accompanying loss of symmetry.

Similar results were noted for the trimethoxysilane precursor, wherein two sharp signals at −54 and −56 ppm merged to form one broad peak at −18 ppm (Figure 5). The greater shift of 36 ppm noted for this sample may be an indication of a greater alteration in the silicon environment in this adduct, for example, the presence of an immobile, cross-linked network. This may result from the formation of mono-, bi-, and tridentate structures, resulting from reactions involving one, two, and three functional groups of a silane molecule with oxygenated species on the nanotube surface, as will be further discussed in more detail later in this work. It is important to note that one can eliminate the possibility that Si−OH is present because the characteristic sharp peak expected at −100 ppm was not observed in any of the spectra.[30] To better probe the exact nature of the chemical change in the SWNTs and the corresponding effect of functionalization on the electronic properties of these tubes, additional spectroscopic methods were employed.

Raman Spectroscopy. Raman spectroscopy is widely used for the characterization of SWNT samples and for gaining information about their structure. It is a particularly powerful probe of electron−phonon coupling and electronic structure in SWNTs. When the incident or scattered photon coincides with an allowed optical transition of a particular nanotube, the Raman spectrum for that tube is considered to be resonantly enhanced. Thus, different lasers bring nanotubes of different diameters into resonance.[31] In this experiment, four excitation wavelengths were used: 488.0 nm (2.54 eV), 514.5 nm (2.41 eV), 632.8 nm (1.96 eV), and 780 nm (1.58 eV). The Raman spectra of the SWNTs measured show three important regions: (a) the radial A_{1g} breathing mode (RBM) mode (in the 100−500 cm^{-1} region) which is dependent on the diameter of the tube that is brought into resonance, (b) the tangential mode, also known as the *G* band in the 1515−1590 cm^{-1} region, which is sensitive to charge exchanged between nanotubes and guest atoms that have intercalated into the interstitial channels in tube bundles, and (c) the disorder mode, the *D* band, which is dispersive in the 1280−1320 cm^{-1} region.[31,32]

i. RBMs. We begin with an analysis of the intensity of the RBM, which depends on the physical and chemical environment of the SWNTs as well as the degree of bundling in the SWNT sample. We also note that the RBMs in observed spectra of the functionalized nanotubes contain a strong component of unreacted tubes, as the signals due to

(28) Duncan, T. M. *A Compilation of Chemical Shift Anisotropies*; Farragutt Press: Chicago, IL, 1990.
(29) Harris, R. K.; Pritchard, T. M.; Smith, E. G. *J. Chem. Soc., Faraday Trans. 1* **1989**, *85*, 1853.
(30) Bauer, F.; Ernst, H.; Decker, U.; Findeisen, M.; Glasel, H.-J.; Langguth, H.; Hartmann, E.; Mehnert, R.; Peuker, C. *Macromol. Chem. Phys.* **2000**, *201*, 2654.
(31) Rao, A. M.; Richter, E.; Bandow, S.; Chase, B.; Eklund, P. C.; Williams, K. A.; Fang, S.; Subbaswamy, K. R.; Menon, M.; Thess, A.; Smalley, R. E.; Dresselhaus, G.; Dresselhaus, M. S. *Science* **1997**, *275*, 187.
(32) Dresselhaus, M. S.; Dresselhaus, G.; Jorio, A.; Souza Filho, A. G.; Pimenta, M. A.; Saito, R. *Acc. Chem. Res.* **2002**, *35*, 1070.

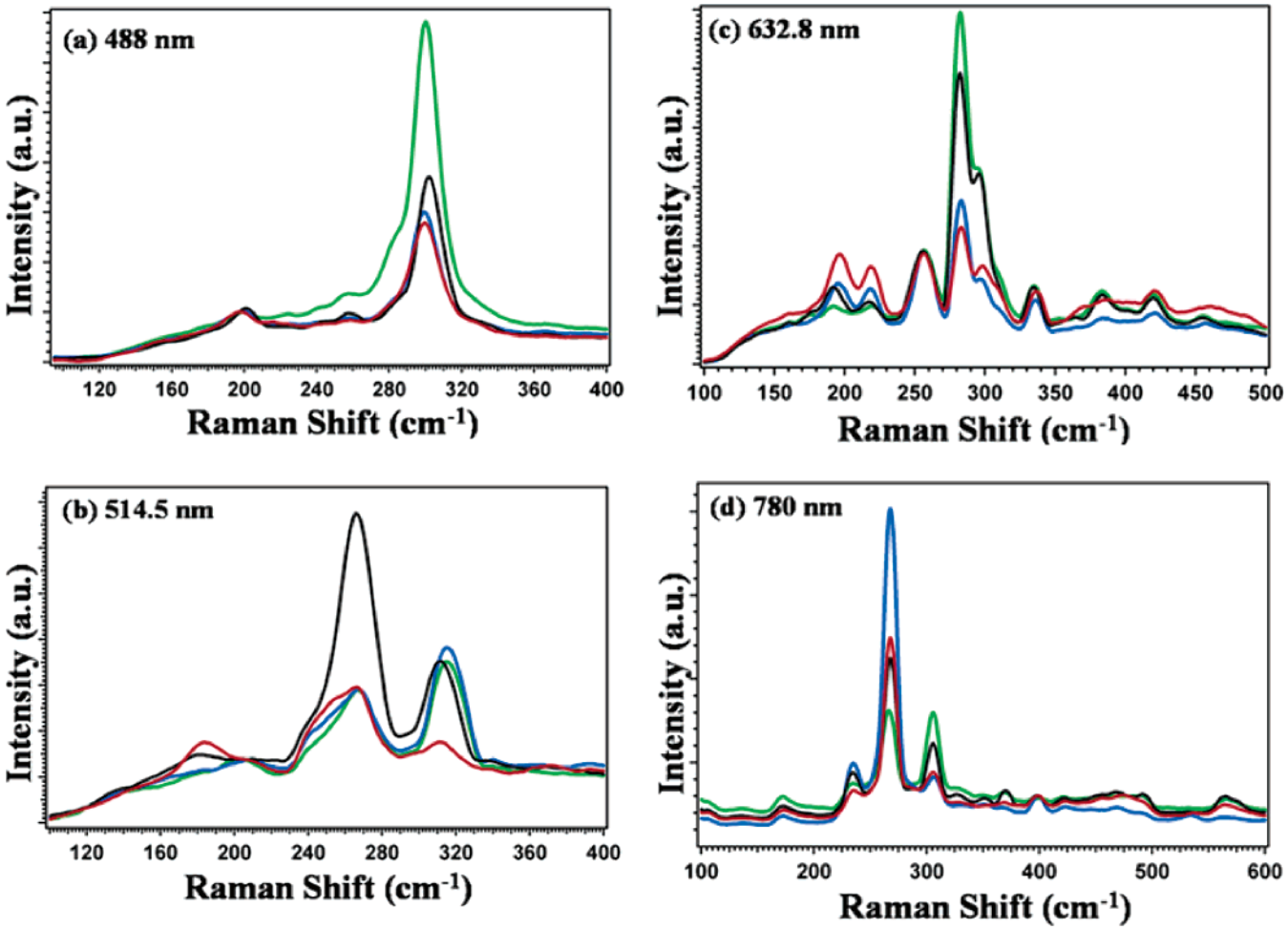

Figure 6. Raman spectra (RBM region) of pristine CoMoCAT SWNTs (black), control samples (green), hexaphenyldisilane−SWNT adducts (blue), and trimethoxysilane−SWNT adducts (red). (a) Excitation at 488 nm with normalization with respect to the RBM feature at 202 cm^{-1}. (b) Excitation at 514.5 nm with normalization with respect to the RBM feature at 208 cm^{-1}. (c) Excitation at 632.8 nm with normalization with respect to the RBM feature at 256 cm^{-1}. (d) Excitation at 780 nm with normalization with respect to the RBM feature at 398 cm^{-1}.

the individually reacted tubes themselves mainly either attenuate in intensity or shift in frequency upon silylation.

The RBM frequency can be empirically related to the diameter of the tube using the equation:

$$\omega_{RBM}\,(cm^{-1}) = 238/d\,(nm)^{0.93} \qquad (1)$$

As a result of the radial nature of the mode in question, the RBM band is particularly affected by the extent of nanotube packing. Hence, to account for the intertube van der Waals interactions,[33] eq 1 incorporates a Lennard-Jones potential in addition to a force constant model.

Excitation at 632.8 nm brings into resonance both metallic and semiconducting tubes. In Figure 6c, a number of RBM features above 240 cm^{-1} arise from semiconducting tubes with diameters ranging from 0.92 to 0.52 nm. These features, located at 256, 283, 296, and 335 cm^{-1}, have been assigned to (10, 3), (7, 5), (9, 2), and (6, 4) nanotubes, corresponding to diameters of 0.92, 0.84, 0.79, and 0.71 nm, respectively.[34] The RBM feature at 192 cm^{-1} has been assigned to (9, 9) metallic nanotubes with an average diameter of 1.22 nm. For trimethoxysilane−SWNT adducts, the larger diameter features are greatly enhanced in intensity upon functionalization, whereas the smaller semiconducting tubes show the opposite trend. Specifically, tubes measuring 0.84 and 0.79 nm in diameter, corresponding to (7, 5) and (9, 2) tubes, respectively, have shown a dramatic decrease in intensity, progressing from the pristine tubes to their functionalized analogues. Thus, it is believed that the trimethoxysilane precursor showed preferential reactive selectivity for semiconducting tubes measuring 0.84 and 0.79 nm in diameter, with correspondingly less reactivity toward metallic nanotubes.

In analyzing the nature of hexaphenyldisilane−SWNT adducts, it can be concluded that this reaction was less diameter-selective. That is, there was a uniform decrease in RBM intensity for features associated with semiconducting nanotubes, an observation indicative of the reactivity of these tubes. However, simultaneously, larger-diameter metallic features showed a slight increase in intensity as compared with those of pristine SWNTs, suggestive of some degree

(33) Rols, S.; Righi, A.; Alvarez, L.; Anglaret, E.; Almairac, R.; Journet, C.; Bernier, P.; Sauvajol, J. L.; Benito, A. M.; Maser, W. K.; Munoz, E.; Martinez, M. T.; de la Fuente, G. F.; Girard, A.; Ameline, J. C. *Eur. Phys. J. B* **2000**, *18*, 201.

(34) Jorio, A.; Santos, A. P.; Ribeiro, H. B.; Fantini, C.; Souza, M.; Vieira, J. P. M.; Furtado, C. A.; Jiang, J.; Saito, R.; Balzano, L.; Resasco, D. E.; Pimenta, M. A. *Phys. Rev. B* **2005**, *72*, 075207.

of preferential enhancement in the resultant silylated product though the degree to which this occurred was not as great as that observed for the trimethoxysilane−SWNT adduct. Evidently, our results suggest that hexaphenyldisilane reacted to a certain extent with metallic tubes in addition to semiconducting tubes, a conclusion also supported by UV−visible spectroscopy, presented later in this work.

Excitation at 514.5 nm (Figure 6b), which probes primarily both smaller-diameter metallic and larger-diameter semiconducting tubes, also evinced similar trends, particularly for the trimethoxysilane-SWNT adduct. That is, for the trimethoxysilane adduct, a band at 312 cm^{-1}, ascribed to 0.76 nm diameter (6, 5) semiconducting tubes, decreased significantly in intensity, while signals at 184 cm^{-1}, associated with metallic tubes measuring 1.31 nm in diameter, increased in intensity, implying preferential reactivity for semiconducting tubes. By contrast, from the selective decrease in intensity observed in the lower wavenumber RBM modes (i.e., at 184 cm^{-1}), the nanotube adduct, associated with hexaphenyldisilane, showed preferential reactivity of metallic tubes as compared with semiconducting tubes.

The results of excitation at 488 nm, probing primarily metallic tubes, are shown in Figure 6a. It is not exactly evident why the relative intensity of a (9, 2) semiconducting nanotube with a diameter of 0.79 nm, as represented by the 302 cm^{-1} peak, increased in the control spectra relative to data associated with the SWNT starting material. Nonetheless, a similar trend, namely, the observation of the preferential reactivity of the semiconducting tubes, for all of these functionalized adducts was observed herein, as well as for data collected at the other excitation wavelengths. That is, in general, a decrease in intensity for the Raman signal associated with functionalized adducts as compared with pristine CoMoCAT SWNTs was noted. In addition, a decrease in the signal at 305 cm^{-1} associated with smaller-diameter (8, 3) semiconducting tubes, measuring 0.78 nm in diameter, was observed for both adducts upon excitation at 780 nm, resonant with $\upsilon 2 \rightarrow c2$ transitions of semiconducting tubes (Figure 6d). Thus, it may be concluded from all of these data that whereas reaction with the hexaphenyldisilane precursor was selective for both smaller-diameter semiconducting and metallic nanotubes, the trimethoxysilane precursor was selective for reaction with certain smaller-diameter semiconducting nanotubes, ranging between 0.76 and 0.84 nm in diameter.

As mentioned previously, the RBM data are affected by the bundling of the nanotubes in a given sample. Specifically, the peak at 218 cm^{-1} observed at 632.8 nm excitation and the 266 cm^{-1} peak noted upon excitation at both 514.5 and 780 nm can provide information about the presence of nanotube bundles.[35,36] We observed contrasting behavior among the different types of nanotubes, which may be due to some extent to consequences arising from the effect of UV irradiation. For instance, a slight decrease in the peak intensity for the control samples at 218 cm^{-1} upon 632.8 nm excitation from Figure 6c, relative to that of pristine CoMoCAT tubes, may indicate very slight de-bundling as a result of the UV irradiation. By contrast, as a result of functionalization with silane derivatives, it is likely that the increase in intensity of the 218 cm^{-1} peak for the adducts as compared with pristine CoMoCAT samples may be attributable to a bundling effect. The apparent decrease in intensity observed for the 266 cm^{-1} peak at 514.5 nm irradiation has also been ascribed to a debundling effect.[35,36] By the same token, the apparent increase in intensity observed for the 266 cm^{-1} peak at 780 nm excitation is consistent with bundling of semiconducting tubes (e.g., (7, 6) tubes).

A complicating factor is that the samples were in solid form while under Raman analysis. It is expected that, in solution, the presence of tubular bundles and the extent of debundling will likely vary from that of solid samples as a result of varying intertube interactions induced by effects such as solvation and sonication.

ii. D and G Bands. The tangential *G* band mode, appearing in the 1400−1700 cm^{-1} region, is related to the Raman allowed phonon mode, E_{2g}, and involves out-of-phase intralayer displacements of the graphene structure of the nanotubes. The *G* band provides information about the electronic properties of carbon nanotubes. The disorder *D* band at around 1350 cm^{-1} is related to the presence of defects as well as nanoparticles and amorphous carbon and usually provides an indication of the level of disordered carbon.

We have used the expression $1 - D/G$, incorporating the ratio of the *D* band intensity to the *G* band intensity, as a measure of nanotube purity, in a fashion similar to protocols utilized by other research groups (Table 1).[37−39] For instance, a low concentration of carbonaceous impurities or imperfections in carbon nanotube samples can be represented by a number close to one. For example, SEM, AFM, and HRTEM data show that pristine nanotubes used in these experiments are relatively pure. For example, at 632.8 nm excitation (Figure 7c), a value of 0.91 was obtained for the pristine samples, while a value of 0.93 was observed for control samples. This slight improvement in sample quality may be attributed to the simple removal of carbonaceous impurities upon exposure to UV lamp irradiation. In addition, this is further indication, along with TEM data, that carbon nanotubes were neither destroyed nor seriously sidewall etched by exposure to UV irradiation alone. It should be noted that the smallest laser power density possible was used during these experiments to prevent damage to the nanotubes.

Calculated values of the expression $1 - D/G$, incorporating the D/G intensity ratio, are shown in Table 1, demonstrating similar trends for all excitation wavelengths utilized. It is evident that this expression decreases upon chemical functionalization, that is, silylation. Moreover, the trimethoxysilane−SWNT adduct showed the smallest value of this

(35) Karajanagi, S. S.; Yang, H.; Asuri, P.; Sellitto, E.; Dordick, J.; Kane, R. S. *Langmuir* **2006**, *22*, 1392.
(36) (a) Heller, D. A.; Barone, P. W.; Swanson, J. P.; Mayrhofer, R. M.; Strano, M. S. *J. Phys. Chem. B* **2004**, *108*, 6905. (b) Hennrich, F.; Kropke, R.; Lebedkin, S.; Arnold, K.; Fischer, R.; Resasco, D. E.; Kappes, M. M. *J. Phys. Chem. B* **2005**, *109*, 10567.
(37) Chen, Z.; Ziegler, K. J.; Shaver, J.; Hauge, R. H.; Smalley, R. E. *J. Phys. Chem. B* **2006**, *110*, 11624.
(38) Dillon, A. C.; Parilla, P. A.; Alleman, J. L.; Gennett, T.; Jones, K. M.; Heben, M. J. *Chem. Phys. Lett.* **2005**, *401*, 522.
(39) Vivekchand, S. R. C.; Jayakanth, R.; Govindaraj, A.; Rao, C. N. R. *Small* **2005**, *10*, 920.

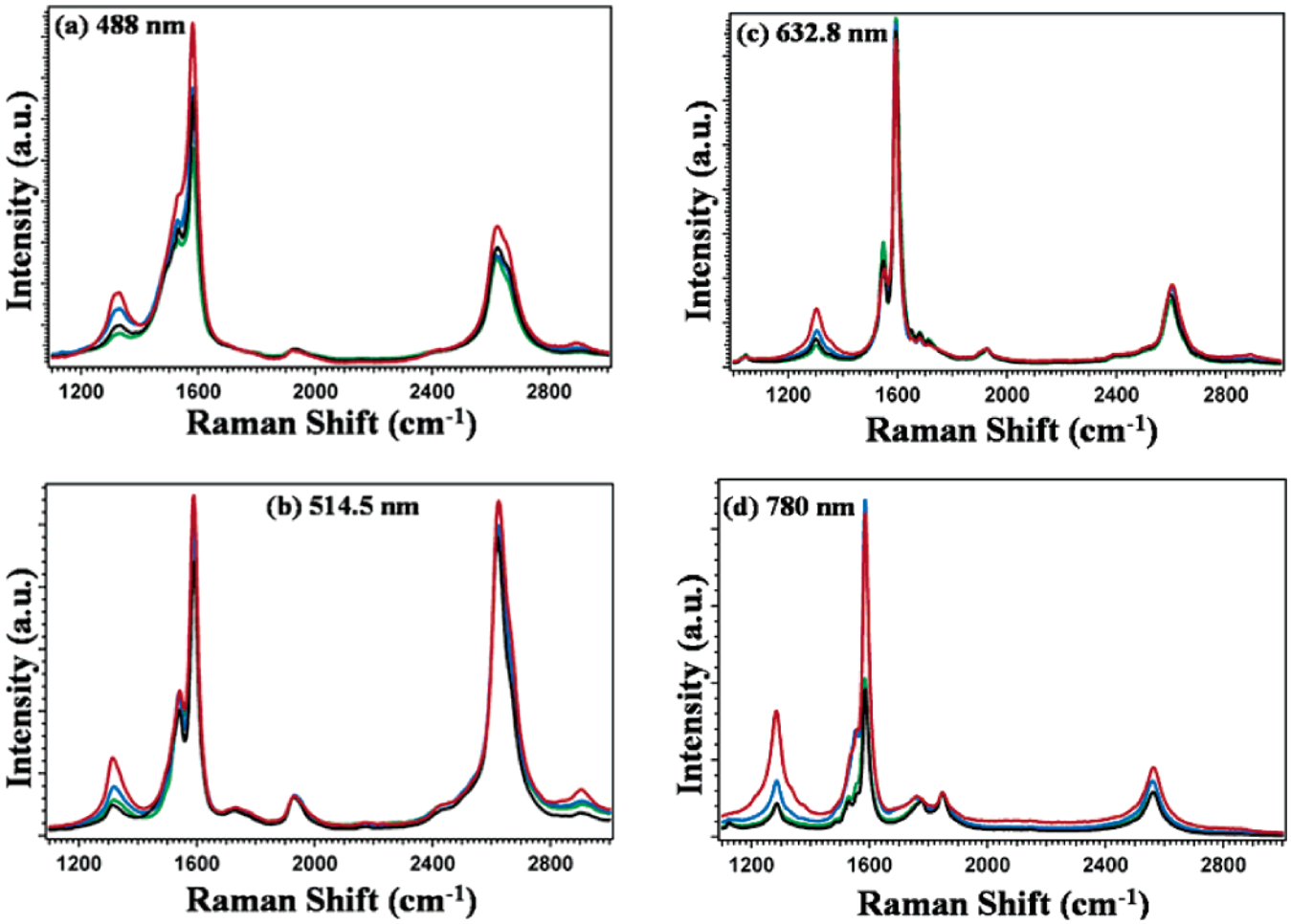

Figure 7. Raman spectra (*D* band, *G* band, and *G*′ band regions) for pristine CoMoCAT SWNTs (black), control samples (green), hexaphenyldisilane−SWNT adducts (blue), and trimethoxysilane−SWNT adducts (red). Normalization was performed with respect to the feature at around 1940 cm^{-1}. Excitation wavelength at (a) 488 nm, (b) 514.5 nm, (c) 632.8 nm, and (d) 780 nm.

Table 1. Mathematical Expression 1 − *D*/*G*, Incorporating the Ratio of the Actual *D* and *G* Band Intensities of Carbon Nanotube Samples Probed at Different Excitation Wavelengths[a]

	excition wavelengths			
sample	488 nm	514 nm	633 nm	780 nm
pristine SWNTs	0.846	0.889	0.914	0.773
control SWNTs	0.850	0.890	0.935	0.802
HPD adduct	0.793	0.839	0.894	0.832
TM adduct	0.785	0.770	0.821	0.610

[a] HPD, hexaphenyldisilane−SWNT adduct, and TM, trimethoxysilane-SWNT adduct.

expression, implying a greater increase of the *D* band intensity (and, hence, greater disorder) relative to hexaphenyldisilane. These results suggest a more effective sidewall functionalization reaction of SWNTs with trimethoxysilane as compared with hexaphenyldisilane, likely through the mediation of added functional groups and extended reactivity at defect sites.

Analysis of the tangential band offers a method for distinguishing between metallic and semiconducting SWNTs. That is, the peak at 1590 cm^{-1} is associated with a diameter-independent G^+ component with A/E_1 symmetry. Peaks at 1560 and 1530 cm^{-1} can be respectively associated with the diameter-dependent G^- component for larger-diameter metallic carbon nanotubes (G_M^-) and with smaller-diameter semiconducting carbon nanotubes (G_S^-) possessing either A or E_1 symmetry.[40] Based primarily on data obtained upon excitation at 488 and 780 nm, in general, we noted that peaks corresponding to the G_S^- signal either decreased in intensity or broadened upon silylation relative to the G_M^- peak profile, whereas the G_M^- feature itself was still prominent. This effect was more pronounced for the trimethoxysilane precursor. In conjunction with the RBM data discussed previously, these results further confirm that the trimethoxysilane precursor has a greater selectivity for semiconducting nanotubes, ranging around 0.8 nm in diameter.

The strong peak at around 2600 cm^{-1} is known as the *G*′ band in graphite and carbon nanotubes, corresponding to the overtone mode of the *D* band.[41] The origin of the *G*′ band has been theoretically shown as a double resonance, two-phonon Raman process which is independent of the presence of defects.[42] Changes in the intensity of this peak should be directly related to the *D* band, which is in fact observed. In

(40) Chou, S. G.; Ribeiro, H. B.; Barros, E. B.; Santos, A. P.; Nezich, D.; Samsonidze, G. G.; Fantini, C.; Pimenta, M. A.; Jorio, A.; Plentz Filho, F.; Dresselhaus, M. S.; Dresselhaus, G.; Saito, R.; Zheng, M.; Onoa, G. B.; Semke, E. D.; Swan, A. K.; Unlu, M. S.; Golberg, B. B. *Chem. Phys. Lett.* **2004**, *397*, 296.
(41) Hishiyama, Y.; Irumano, H.; Kaburagi, Y. *Phys. Rev. B* **2001**, *63*, 245406.
(42) Saito, R.; Jorio, A.; Souza Filho, A. G.; Dresselhaus, G.; Dresselhaus, M. S.; Pimenta, M. *Phys. Rev. Lett.* **2002**, *88*, 027401.

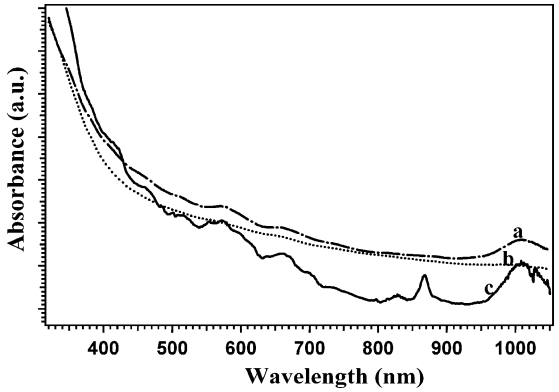

Figure 8. UV−visible spectra of (a) trimethoxysilane−SWNT adducts (dashed-dotted line); (b) hexaphenyldisilane−SWNT adducts (dotted line); and (c) control samples (solid line).

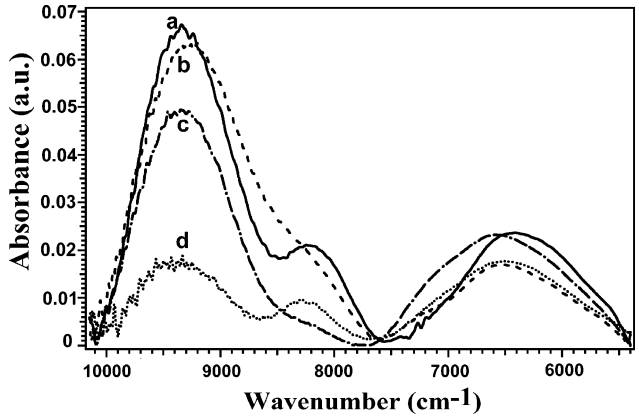

Figure 9. Near-IR spectra of (a) pristine CoMoCAT pristine SWNTs (solid line); (b) hexaphenyldisilane−SWNT adducts (dashed line); (c) control sample (dashed-dotted line); and (d) trimethoxysilane−SWNT adducts (dotted line).

most cases, there was an increase in intensity observed for the functionalized adducts as compared with the pristine CoMoCAT samples. Shifts of this band have been previously correlated with changes in bond strength upon functionalization.[43] We cannot rule out the presence of bundling or of localized changes in purity as contributive factors toward explaining our data.

UV−Vis−NIR Data Interpretation. Allowable transitions between van Hove singularities in the electronic density of states of SWNTs are observable as spike-like features in the optical spectra of nanotube thin films and solutions.[44−46] These transitions usually occur in the UV−visible−near-IR region with their exact position determinant on the diameter of the nanotubes analyzed.[47] Only a few sharp absorption peaks were observed in the entire UV−visible−NIR spectrum (Figures 8 and 9). Bands corresponding to the metallic SWNTs (350−600 nm) were much weaker than those of the semiconducting nanotubes (550−1400 nm). It should be noted that the UV−visible data were collected from solutions and dispersions, obtained by sonication of SWNT samples in DMF followed by centrifugation.[48] It also should be emphasized that although surfactants such as sodium dodecyl sulfate are very effective at exfoliating tube bundles, it is still possible to observe transitions in the UV−visible region upon simple sonication in DMF, as was performed in previous reports.[48]

Because SWNTs prepared by most bulk synthesis methods occur as ropes of nanotubes held together by van der Waals forces, their corresponding absorption spectra appear as broad peaks which are, in fact, an aggregate superposition of the absorption spectra of individualized nanotubes of many different diameters and chiralities. Previous reports suggest that there is no preferential suspension of any specific nanotube type upon sonication of pristine CoMoCAT tube samples, because all observed peak intensities increased simultaneously during sonication.[49]

Figures 8 and 9 represent a comparison of CoMoCAT pristine SWNTs, of control samples, and of two silane-treated SWNT adducts in the UV−vis−NIR range. From Figure 8, in general, it can be concluded that both metallic and semiconducting nanotubes were covalently sidewall functionalized by hexaphenyldisilane, an observation supported by the disappearance of all of the electronic transitions in plot b, with respect to the controls. This loss of transitions in the UV range is indicative of covalent sidewall functionalization, which disrupts the electronic structure of nanotubes. Thus, it is hypothesized that silylation essentially saturates the bond structure on the nanotube sidewalls and introduces defects that perturb and destroy the intrinsic periodicity of the conjugated sp^2-hybridized nanotube electronic structure.[50]

The reaction with trimethoxysilane demonstrated a more selective sidewall functionalization for specific semiconducting nanotubes. This was implied from the conservation of metallic features (Figure 8, plot a) after functionalization, indicative of minimum reactivity toward these tubes. Specifically, there was likely selective functionalization of (6, 4) semiconducting tubes, measuring 0.71 nm in diameter, as demonstrated by the complete disappearance of the 868 nm peak. In addition, the peak at 828 nm, corresponding to (5, 4) semiconducting tubes, measuring 0.62 nm in diameter, also diminished in intensity.[51] Features at 1008 and 567 nm, which can be ascribed to the S_{11} and S_{22} transitions, respectively, of (6, 5) semiconducting tubes of diameter 0.76 nm, also decreased to some extent in intensity, indicative of their intrinsic reactivity, corroborating the Raman data discussed previously. Thus, taken collectively, these spectroscopic results strongly suggest that the reaction with trimethoxysilane is particularly selective for certain smaller diameter semiconducting nanotubes including but not limited to those measuring in the range of 0.62, 0.71, 0.76, 0.79, and 0.84 nm in diameter, while hexaphenyldisilane is reactive toward both semiconducting and metallic nanotubes ranging

(43) McGuire, K.; Gothard, N.; Gai, P. L.; Dresselhaus, M. S.; Sumanasekera, G.; Rao, A. M. *Carbon* **2005**, *43*, 219.
(44) Chen, J.; Hamon, M. A.; Hu, H.; Chen, Y.; Rao, A. M.; Eklund, P. C.; Haddon, R. C. *Science* **1998**, *282*, 95.
(45) Wildoer, J. W. G.; Venema, L. C.; Rinzler, A. G.; Smalley, R. E.; Dekker, C. *Nature* **1998**, *391*, 59.
(46) Bachilo, S. M.; Balzano, L.; Herrera, J. E.; Pompeo, F.; Resasco, D. E.; Weisman, R. B. *J. Am. Chem. Soc*. **2003**, *125*, 11186.
(47) Zhang, L.; Balzano, L.; Resasco, D. E. *J. Phys. Chem. B* **2005**, *109*, 14375.
(48) Buffa, F.; Hu, H.; Resasco, D. E. *Macromolecules* **2005**, *38*, 8258.
(49) Tan, Y.; Resasco, D. E. *J. Phys. Chem. B.* **2005**, *109*, 14454.
(50) Kamaras, K.; Itkis, M. E.; Hu, H.; Zhao, B.; Haddon, R. C. *Science* **2003**, *301*, 1501.
(51) Weisman, R. B.; Bachilo, S. M. *Nano Lett.* **2003**, *3*, 1235.

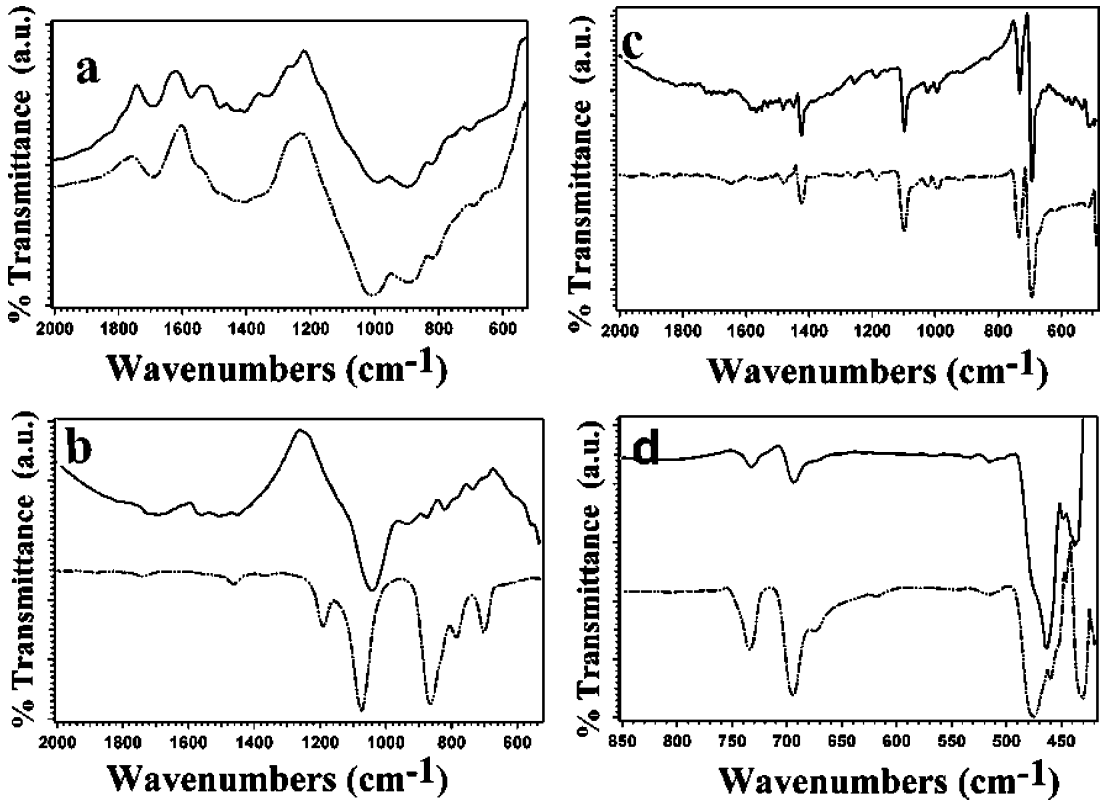

Figure 10. Mid-IR spectra of (a) pristine CoMoCat SWNTs (solid line; upper curve) and of control samples (dashed-dotted line; lower curve); (b) of trimethoxysilane-SWNT adducts (solid line; upper curve) and trimethoxysilane precursor (dashed-dotted line; lower curve); and (c) and (d) of hexaphenyldisilane-SWNT adducts (solid line; upper curve) and hexaphenyldisilane precursors (dashed-dotted line; lower curve) in different wavenumber regions.

below ~1.3 nm. In addition, the presence of more prominent peaks in the trimethoxysilane adduct spectrum suggests a de-bundling effect in solution, which may account for the increased stability of these functionalized tubes in DMF solution (Supporting Information).[35]

In Figure 9, the major bands observed correspond to S_{11} and S_{22} transitions between the first and second pairs of van Hove singularities for semiconducting nanotubes. The band at 9345 cm^{-1} is consistent with that of the S_{22} transitions observed for tubes with calculated diameters close to 1.5 nm of the (15, 7) type.[51] Bands have also been noted at around 8192 and 6423 cm^{-1}, respectively, corresponding to S_{22} and S_{11} transitions of tubes measuring 1.86 and 1.35 nm in diameter, respectively.[51] By comparing the relative intensity of the 9345 and 6423 cm^{-1} peaks, it can be seen that there was selectivity for 1.5 nm semiconducting tubes in the reaction with trimethoxysilane, because the S_{22} peak for these tubes decreased significantly in intensity with respect to the S_{11} transition. By contrast, the reaction with the hexaphenyldisilane did not appear to have obviously disrupted these particular transitions. Thus, again, coupled with a significant weakening of the M_{11} transition, our data support the selectivity of the reaction with the trimethoxysilane precursor for predominantly semiconducting nanotubes.

Mid-IR Data Interpretation. To better understand the chemical nature of the attachment mechanism of silanes onto the SWNT surface, mid-IR spectra were obtained. Mid-IR spectroscopy was used to investigate the identity of functionalities on the carbon nanotube surface. As observed in the spectrum of pristine tubes (Figure 10a), the C═C peak at 1566 cm^{-1} could be attributed to the carbon skeleton in-plane E_{1u} stretch of the nanotubes.[52] Although these nanotubes were not intentionally functionalized with oxygenated groups through a protocol such as an acid treatment, the presence of surface oxygenated functionalities was nonetheless noted. For example, the peak at 1693 cm^{-1} can be assigned to the carbonyl (C═O) stretching vibration, associated with ketones, aldehydes, or carboxylic acid groups, whereas the peak at 1253 cm^{-1} corresponds to a C—O stretch. Other features, such as that at 1000 cm^{-1}, may be attributed to the carbon ring breathing mode and C—H bending. It should also be noted that similar spectral features were observed both in pristine and in control samples. These observations further confirm that spectral band alteration changes, observed with the adduct's IR spectra, likely had chemical origins, associated with the silane reaction itself, as opposed to external, physical stimuli such as exposure to UV irradiation.

Figure 10, part b illustrates spectra for the trimethoxysilane precursor and the trimethoxysilane−SWNT adduct, respectively. The 1457 cm^{-1} peak, representing the antisymmetric methyl deformation, can be observed in both spectra, indicating that methyl groups were still attached to silicon upon coordination to the carbon nanotubes. The 1074 cm^{-1} peak, initially observed in the precursor spectrum, can be ascribed to the Si—O—C stretch and is shifted to 1037 cm^{-1} in the carbon nanotube adduct.[53] In addition, the associated

(52) Hemraj-Benny, T.; Banerjee, S.; Wong, S. S. *Chem. Mater.* **2004**, *16*, 1855.
(53) Lambert, J. B.; Shurvell, H. F.; Lightner, D. A.; Cooks, R. G. *Organic Structural Spectroscopy*; Prentice Hall: Upper Saddle River, NJ, 1998.

peak width increased in magnitude. The Si—O—C deformation peak, initially observed at 787 cm^{-1} in the precursor spectrum, presumably was displaced to 737 cm^{-1} in the adduct spectrum. As the prominent Si—H deformation peak observed at 866 cm^{-1} in the trimethoxysilane precursor spectrum in Figure 10b was significantly reduced in intensity with respect to the corresponding peak region in the adduct spectrum, this result is consistent with the removal of the proton itself upon attachment to the SWNTs. It can also be assumed that no unreacted trimethoxysilane precursor was present in the adduct sample, because no discernible Si—H peak at 866 cm^{-1} was observed in the adduct spectrum. In addition, the fact that a Si—O—C peak was noted in the adduct spectrum suggested that hydrolysis of the methoxy groups likely did not occur. Moreover, to confirm this point, no Si—OH vibrations at 798 and 956 cm^{-1} were detected, as noted in previous reports.[19]

Spectra in Figure 10, parts c and d, represent the hexaphenyldisilane precursor and the hexaphenyldisilane—SWNT adduct, respectively, in two complementary spectral ranges. The first conclusion that can be drawn from the plots in part c is that most of the features noted in the precursor spectrum can be seen in the corresponding adduct. Specifically, the 1484 cm^{-1} peak represents the aromatic ring C═C stretch of the phenyl rings, whereas the 1190 and 732 cm^{-1} peaks represent the C—H in-plane bending and out-of-plane bending, respectively.[53] In addition, a very sharp 695 cm^{-1} peak can be attributed to out-of-plane C—H deformations of the phenyl rings. Because these features can be observed for both the hexaphenyldisilane precursor and its corresponding functionalized adduct, one can assume that if in fact the silane precursor is attached to the carbon nanotube surface, the phenyl groups remain effectively attached to the silicon atom. That is, the hexaphenyldisilane precursor did not totally fragment. Additional evidence for this assertion can be corroborated by the presence of Si—C stretch signals at 1257 cm^{-1} and at 1099 cm^{-1} in both spectra.

Mid-IR evidence also indicated the cleavage of the Si—Si bond, as can be seen in Figure 10, part d, where the Si—Si bond[54] peak at 430 cm^{-1} decreased significantly with respect to that of the 475 cm^{-1} peak. The 475 cm^{-1} peak, representing the in-plane and out-of-plane ring deformations,[53] shifted slightly downfield with a change in its features. These observations are consistent with the idea of attachment of molecules to the carbon nanotube sidewalls and associated defect sites. It should also be noted that features such as the C═C stretch at 1566 cm^{-1} for the carbon nanotube framework were observed in the spectra of both the pristine material and its associated silylated nanotube adduct and that silicon dioxide was not detected.

XPS Analysis. To further confirm the above data, XPS was used to provide information about the chemical composition and bonding of the carbon nanotube—silane adducts. Table 2 shows the estimated atomic concentration of carbon, oxygen, and silicon in the starting materials and in the associated adducts.

(54) Nakamato, K. *Infrared and Raman Spectra of Inorganic and Coordination Compounds*, 5th ed.; John Wiley & Sons: Canada, 1997, Part A.

Table 2. XPS Data of the Estimated Atomic Concentrations (in %) of Species Attached to SWNTs within a 2−4 nm Top Surface Analyzed Layer[a]

	estimated atomic concentrations (%)		
sample	C	O	Si
CoMoCAT SWNTs	78.67	11.20	2.22
control SWNTs	89.14	5.19	
HPD adduct	87.24	10.54	1.55
TM adduct	52.29	34.36	7.29

[a] HPD, hexaphenyldisilane—SWNT adduct, and TM, trimethoxysilane-SWNT adduct.

As confirmed by IR data, there were a number of oxygenated functionalities such as C—O, C═O, and O—C═O groups present on the surfaces of CoMoCAT nanotubes. Exact percentages are presented in Supporting Information. The increased oxygen concentration observed for the trimethoxysilane—SWNT adducts can be attributed to the presence of the silane derivative. In addition, there was silicon present in the initial CoMoCAT carbon nanotube sample. After base treatment, the sample silicon content decreased to an estimated zero percent, as previously suggested by EDS. Thus, the presence of silicon in the functionalized adduct could be associated with the silane derivative, as predicted.

Hence, based on the mid-IR data and the XPS high-resolution data (Supporting Information), it can be concluded that with the trimethoxysilane—SWNT adduct, the precursor could attach to the carbon nanotube surface by means of oxygenated groups, through which a Si—O—Si scaffolding framework and associated coating could form. In other words, as suggested by XPS, the binding energy of 100.61 eV can be attributed to the actual binding of SiO to the carbon nanotube ($SiO—C_{NT}$), whereas the binding energy at 103.30 eV can be plausibly ascribed to a siloxane network (Si—O—Si).[20] Although it is possible that the methyl groups were completely removed in the reaction, it is known from mid-IR data that some of the methyl groups were still present in the functionalized adduct. Hence, the shift and broadening in the Si—O—C peak observed in the adduct could actually have been attributed to the presence of two types of Si—O—C bonding, namely, a Si—O—C bond in the precursor as well as a $Si—O—C_{NT}$ bond. In the latter case, methyl groups were removed, allowing the oxygen to react with the C═C carbon nanotube framework. There is nothing to discount the possibility of the trimethoxysilane precursor itself undergoing bonding with the Si—O—Si surface. This scenario is in agreement with observations noted in ^{29}Si NMR data, implying the formation of mono-, bi-, and tridentate structures, resulting from reactions involving one, two, and three functional groups of a silane molecule with oxygenated species on the nanotube surface. In addition, the increase in the Raman D band intensity observed for the adducts is consistent with this type of attack of the C═C framework.

The reaction of SWNTs with hexaphenyldisilane was likely somewhat milder with cleaving of the reagent molecule followed by attachment through the spatially limited oxygen-decorated ends and defect sites of the nanotubes. Similar to the trimethoxysilane adduct, a peak corresponding to a binding energy of 100.92 eV was observed and could be attributed to the binding of SiO to the carbon nanotube

Scheme 2. Schematic Representation, Not Drawn to Scale, of the Carbon Nanotube Framework (CNT) with Attached Silane Precursors[a]

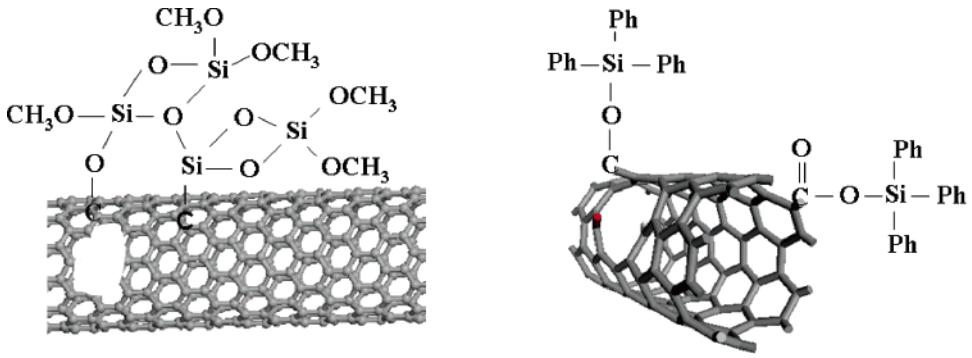

(a) Trimethoxysilane adduct **(b) Hexaphenyldisilane adduct**

[a] (a) Trimethoxysilane adduct demonstrating dominance of Si—O—Si network along with the presence of $-Si(OCH_3)_n$ groups forming a coating. (b) Hexaphenyldisilane adduct demonstrating attachment of $-Si(Ph)_3$ groups to oxygenated functionalities onto the ends and defect sites of the nanotube. Phenyl groups are represented by Ph.

($SiO-C_{NT}$). As the UV−visible data indicated, there was a degree of perturbation of the electronic structure as a result of sidewall functionalization, but the slight increase in the D band in the Raman data suggested this was not overly significant. Consistent with the mid-IR data, phenyl groups arising from the reagent were still present in the SWNT adduct upon attachment.

Conclusions

A proposed mechanism of attachment of the individual silane precursors can be postulated on the basis of the analysis presented above. Specifically, for the trimethoxysilane adduct, it can be assumed that the proton was removed by the platinum catalyst, activated by the UV irradiation allowing attachment (to some extent) of the $-Si(OCH_3)_3$ not only to (1) the carbon nanotube C═C framework but also to (2) oxygenated functionalities onto the ends as well as defect sites along the sidewalls on the nanotube framework. On the basis of the XPS and NMR data, a loss of the methyl groups from the precursor would allow for formation of an intermolecular —Si—O—Si— network with the attached —SiO groups forming the coating observed by microscopy. The presence of this coating may also account for the increased solubility and stability observed for this adduct as compared with the adduct derived from the hexaphenyldisilane reaction. A proposed representation of this reaction schematic can be observed in Scheme 2.

By comparison, for the hexaphenyldisilane adduct, XPS data suggested the likelihood of Si attachment to the carbon nanotube framework, more specifically to the oxygenated functionalities at the ends and defect sites of the nanotubes. Therefore, it can be hypothesized, as also corroborated by IR and NMR data, that the Si—Si bond breaks upon UV irradiation to facilitate attachment of the $-Si(Ph)_3$ groups to the oxygenated groups on the nanotube framework. Possible scenarios regarding moiety attachment are noted in Scheme 2.

In general, it can be concluded that the SWNTs can be effectively silylated with both trimethoxysilane and hexaphenyldisilane precursors. The trimethoxysilane precursor was selectively more reactive toward semiconducting nanotubes than metallic nanotubes. This observation is likely a consequence of the fact that the majority of semiconducting nanotubes observed, as we have shown through Raman data in particular, possessed generally smaller diameters. These results are consistent with our initial expectation that smaller-diameter tubes would be more reactive than larger-diameter tubes toward silylation. The fundamental point to note is that coatings of dielectric materials can be placed onto SWNT ends and sidewalls through a well-defined, relatively mild molecular reaction, which is structurally nondestructive to the nanotube itself.

Acknowledgment. Acknowledgment is made to the National Science Foundation (DMII -0403859 and DMR-0348239) and to the donors of the Petroleum Research Fund, administered by the American Chemical Society, for support of this research. The authors thank Dr. Mandakini Kanungo, Dr. James Quinn, and Dr. Yuanbing Mao for assistance with AFM, SEM, and HRTEM analyses, respectively. Dr. Drew Hirt (Materials Analytical Services) and Dr. Zhorro Nikolov (Drexel University) are thanked for their help with collection of the XPS and Raman data, respectively. The authors are also grateful to Dr. Boris Itin (New York State Structural Biology Center) and to Dr. Martine Ziliox for their expert assistance with our silicon NMR data. S.S.W. is an affiliated member of the New York Structural Biology Center, a STAR center supported by the New York State Office of Science, Technology, and Academic Research. NMR resources are supported by NIH P41 GM66354.

Supporting Information Available: XPS data for pristine CoMoCAT SWNTs, control samples, hexaphenyldisilane−SWNT adducts, and trimethoxysilane−SWNT adducts and photographs showing solubility in DMF of trimethoxysilane−SWNT adducts, control samples, and hexaphenyldisilane−SWNT adducts as well as stability in DMF of trimethoxysilane−SWNT adducts, control samples, and hexaphenyldisilane−SWNT adducts, after 2 weeks (PDF). This material is available free of charge via the Internet at http://pubs.acs.org.

CM061185X